Application of Radio Ground-Wave Propagation Theory to the Tomographic Imaging of Ground Surfaces

Zhipeng Wu, *Member, IEEE*

***Abstract*—Radiowave propagation over ground has been historically studied for predicting the radiated fields when the ground properties are known and the field has been well covered over the past hundred years. In this paper, the theory of ground wave propagation is applied to inverse problem of the tomographic imaging of ground surfaces. After the inverse problem is formulated, an iterative technique for solving it is illustrated. This is based on the minimization of the cost function of the measured and estimated scattered fields produced by the surface under investigation in isolation. Numerical simulation results are presented for the reconstruction of four different ground features surrounded by sea water namely: 1) dry ground; 2) wet ground; 3) dry–wet mixed ground; and 4) dry ground with a central water pool. It has been demonstrated that the technique is able to reconstruct the distributions of normalized surface impedance of the isolated surfaces and, hence, their images. The iterative process can converge with a small number of iterations using the normalized surface impedance of sea water as the initial guessed values. However, better images can be produced using *a priori* information. This study thus illustrates a new application of ground wave propagation theory with possible applications in ground surface mapping, remote sensing, target positioning and monitoring, and navigation.**

***Index Terms*—Electromagnetic (EM) tomography, ground-wave propagation.**

I. Introduction

RADIOWAVE propagation over the ground surface of the earth at low, medium, and high frequencies has been studied theoretically and experimentally over the past hundred years [1], [2]. In obtaining the solutions to these problems, a number of different models and assumptions are made in order to obtain simplified solutions. A current element is usually considered as the radiation source, although other sources are also used. Historically, the ground was first modeled to be flat and homogeneous for short propagation ranges [3]–[11] and spherical in shape for long distance propagation [12]–[17]. Ground surface inhomogeneity and irregularity was then introduced in the model to take into account the effects of mixed path propagation, and irregular terrain [18]–[44]. The electric and magnetic fields from the radiation of a current element over a flat homogeneous ground were thus expressed in closed form and those over a spherical ground in the sum of a residue series. However, for inhomogeneous or irregular grounds, the radiated fields were usually given in the form of an integral equation for the attenuation function, which could be derived from either the compensation theorem [20], [43]–[46] or Green's theorem [18], [19], [23], [39]–[42], [47], [48]. This integral equation could be solved to give numerical solutions, which have been confirmed experimentally to be accurate at low, medium, and high frequencies. The subject of theoretical radiowave propagation over a ground surface is, thus, now reasonably well understood and tested as a forward problem.

However, as the radiated fields and ground properties are related by the same set of equations, measurements of the fields can be used to determine the ground properties. This is inverse problem. With the use of multiple fixed transmitting and receiving antennas, or a portable transmitter and a portable receiver, to create "multiviews" of the ground surface, as in X-ray or microwave tomographic systems [49], [50], the ground surface can be mapped in terms of its impedance properties. Consequently, the image of the ground surface can be reconstructed. The resolution of this image will depend on the operating frequency. When the area under imaging is discretized, the resolution would further depend on the size of the cell, which is usually chosen to be in the range between $\lambda/20$ and $\lambda/10$. A higher operating frequency and smaller cell area would give a better resolution. However, the use of a higher frequency would require a larger number of discretized cells per square wavelength and, thus, demand more computing capacity. A compromise between the resolution and computing requirement would be the choice of a frequency at which the diameter of the area to be imaged is the order of a wavelength in free-space. For the imaging of a ground surface of diameter of the order of a few hundred meters or kilometers, a frequency in the medium or high-frequency band would be most suitable. Hence, such frequency bands will be considered in this paper for tomographic imaging of ground surfaces. In the following sections, the technique for producing tomographic images of ground surfaces will be presented.

In Section II, the forward problem of radiowave propagation over ground will be described by considering an isolated ground such as an island surrounded by seawater. In Section III, the inverse problem will be formulated to provide the procedure for obtaining the dielectric constant distribution from the measurements of the scattered fields from this isolated ground surface. Finally, numerically simulated results of the image reconstruction for a number of isolated ground features will be presented in Section IV.

Manuscript received September 26, 1999; revised April 5, 2000.

The author is with the Department of Electrical Engineering and Electronics, University of Manchester Institute of Science and Technology, Manchester M60 1Q, U.K. (e-mail: wu@fs5.ee.umist.ac.uk).

Publisher Item Identifier S 0018-926X(00)09340-6.

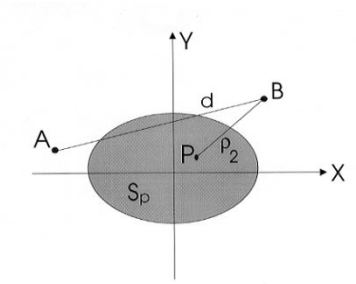

Fig. 1. Radiation of a vertical current element at A over an isolated surface

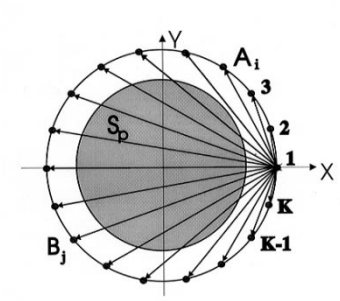

Fig. 2. Measurement configuration to create multiviews of the isolated surface

II. Formulation of the Forward Problem of Radiowave Propagation over an Isolated Surface

The consideration of an isolated surface for imaging purposes does not lose its generality as the largest contribution to the attenuated fields arises from the first Fresnel zone. The propagation of radiowaves over an isolated surface, as shown in Fig. 1, can be formulated using the compensation theorem [45], [46] or Green's theorem [47], [48]. The two methods lead to slightly different expressions for the attenuation function [31], [32], [34], [36], [38]. Here, the scalar Green's theorem, which was used by Feinberg *et al.* [18], [19], [23], [39]–[41] in dealing with irregular terrain, will be used. The transmitting antenna is considered to be a vertical electric current element $I_1\,dl$ located at A on the ground surface. Following the work given in [51], [52], the vertical electric field component $E_{z1}(B)$ at the receiving point B on the ground surface can be written as

$$E_{z1}(B) = E^0_{z1}(B) + E^s_{z1}(B) \tag{1}$$

where

- subscript 1 — field produced by the current element $I_1\,dl$;
- $E^0_{z1}(B)$ — vertical electric field component at B from the radiation of the same current element $I_1\,dl$ on a homogeneous ground with a constant normalized surface impedance Δ_0;
- $E^s_{z1}(B)$ — scattered vertical electric field component at B due to the isolated inhomogeneity.

$E^0_{z1}(B)$ is given by

$$E^0_{z1}(B) = A_{PG} F(w_{1B}) \frac{e^{-jk_0 d}}{d} \tag{2}$$

where

- A_{PG} constant depending on the transmitted power and antenna gain;
- k_0 wave number in free-space;
- d distance between A and B

$$F(w) = 1 - j\sqrt{\pi w} e^{-w} \mathrm{erfc}\left(j\sqrt{w}\right) \tag{3}$$

is the Sommerfeld attenuation function and

$$w_{1B} = -\frac{jk_0 d}{2}\,\Delta_0^2 \tag{4}$$

is the Sommerfeld numerical distance [8]. The scattered field $E^s_{z1}(B)$ in (1) is given by

$$E^s_{z1}(B) = \frac{1}{Z_0 I_2\,dl} \iint_{S_p} [\Delta_s(P) - \Delta_0] E_{z1}(P) E^0_{z2}(P)\,dS \tag{5}$$

where

- Z_0 wave impedance in free-space;
- S_p area of the isolated surface;
- $E_{z1}(P)$ vertical electric field component at P from the radiation of the same current element on the inhomogeneous ground surface with a normalized surface impedance distribution of $\Delta_s(P)$;
- $E^0_{z2}(P)$ vertical electric field component at a point P on the isolated surface from the radiation of a vertical electric current element $I_2\,dl$ at B on a homogeneous ground with a normalized surface impedance Δ_0.

$$E^0_{z2}(P) = -\frac{jk_0 Z_0 I_2\,dl}{2\pi} F(w_{2P}) \frac{e^{-jk_0\rho_2}}{\rho_2} \tag{6}$$

where ρ_2 is the distance between B and P and $F(w_{2P})$ is the Sommerfeld attenuation function with the numerical distance

$$w_{2P} = -\frac{jk_0\rho_2}{2}\,\Delta_0^2. \tag{7}$$

Substituting (6) into (5) gives the following expression for $E^s_{z1}(B)$:

$$E^s_{z1}(B) = -\frac{jk_0}{2\pi} \iint_{S_p} [\Delta_s(P) - \Delta_0] \cdot E_{z1}(P) F(w_{2P}) \frac{e^{-jk_0\rho_2}}{\rho_2}\,dS. \tag{8}$$

Equations (8) and (1) form an integral equation for the total vertical electric field $E_{z1}(B)$, which can be solved numerically when the isolated surface is discretized. The isolated surface could be divided into a number of square cells. For a circular isolated surface, a different scheme as shown in Fig. 2(a) can be employed. The circular surface is divided into N_r rings [$N_r = 5$ in Fig. 2(a)] and $4(2n_r + 1)$ segments in each ring for $n_r = 1$ to N_r, giving a total of $4N_r^2$ cells of equal area. Assuming the isolated surface is divided into a total of N cells of equal surface areas with the use of one-dimensional cell numbering

scheme $n = 1$ to N, the vertical electric field at point B can be approximated by

$$E_{z1}(B) = E^0_{z1}(B) - \frac{jk_0}{2\pi}\sum_{n=1}^{N}[\Delta_{sn} - \Delta_0] \cdot E_{z1,n}F(w_{2n})\iint_{S_n}\frac{e^{-jk_0\rho_2}}{\rho_2}\,dS \tag{9}$$

where Δ_{sn}, $E_{z1,n}$, $F(w_{2n})$ are the values of $\Delta_s(P)$, $E_{z1}(P)$, $F(w_{2P})$ at the nth cell, which are taken to be constant across the cell as an approximation. In (9), ρ_2 is the distance from point B to a point on the nth cell and S_n is the surface of the nth cell. The integration in (9) could be performed using quadrature methods [32]. This however is time consuming. By using the method of approximating the area of each cell by a circle of the same area, which was first proposed by Richmond [53] in dealing with electromagnetic (EM) scattering from dielectric objects, an analytical expression can be obtained. The computation can be simplified further by the use of the spherical harmonic expansion of exponent $(-jk_0\rho_2)/\rho_2$ given in [48], [54] with the choice of the arbitrary origin to coincide with the center of the nth cell, and with $\theta = \pi/2$ and $\theta' = \pi/2$ for points on the ground surface. This gives

$$\iint_{S_n}\frac{e^{-jk_0\rho_2}}{\rho_2}\,dS = -j2\pi k_0\sum_{n'=0}^{\infty}(2n'+1)h^{(2)}_{n'}(k_0\rho_{Bn}) \cdot P_{n'}(0)P_{n'}(0)\int_0^{a_n} j_{n'}(k_0r')r'\,dr' \tag{10}$$

where

$j_{n'}(x)$ and $h^{(2)}_{n'}(x)$	spherical Bessel functions of order n';
$P_{n'}(0)$	Legendre function of the first kind;
$\rho_{B,n}$	distance between point B and the center of the nth cell;
a_n	radius of the circle having the same area as S_n.

A numerical study of the series in (10) shows that for the numerical examples to be presented in Section IV, the first term is at least 30 times larger than the second term which corresponds to $n' = 2$. Keeping the first term as the first-order approximation leads to the closed-form expression

$$\iint_{S_n}\frac{e^{-jk_0\rho_2}}{\rho_2}\,dS = \frac{e^{-jk_0\rho_{Bn}}}{\rho_{Bn}}\,\frac{2\pi}{k_0^2}\,(1-\cos(k_0a_n)) \tag{11a}$$

Alternatively using the physical optics approximation, the distance ρ_2 in the phase term of the left-hand side (LHS) of (10) can be approximated by $\rho_2 \approx \rho_{Bn} - r'\cos(\phi')$. The integration over the equivalent circular area then gives

$$\iint_{S_n}\frac{e^{-jk_0\rho_2}}{\rho_2}\,dS = \frac{e^{-jk_0\rho_{Bn}}}{\rho_{Bn}}\,\frac{2\pi}{k_0^2}\,(k_0a_n)J_1(k_0a_n). \tag{11b}$$

Numerical studies show that (11a) and (11b) provide good approximations to the integration $\iint_{S_n}(e^{-jk_0\rho_2}/\rho_2)\,dS$. The errors are usually less than 1% with (11b) generally giving slightly smaller errors than (11a).

If the point B coincides with the center of the nth cell so that $\rho_{Bn} = 0$, (11a) and (11b) cannot be applied. However, in this case, it can be easily shown that

$$\iint_{S_n}\frac{e^{-jk_0\rho_2}}{\rho_2}\,dS = \frac{2\pi}{jk_0}\,(1-e^{-jk_0a_n}). \tag{11c}$$

By selecting the field point B to be at the center of each cell sequentially from $m = 1$ to N, a set of linear equations can be obtained from (9) for the solution of the electric field distribution on the isolated surface. This can be written in matrix form as

$$[C_{mn}][E_n] = [E^0_m] \tag{12}$$

where $E_m = E_{z1}(B)$ and $E^0_m = E^0_{z1}(B)$ when B is at the center of the mth cell

$$C_{mn} = \frac{e^{-jk_0\rho_{mn}}}{-jk_0\rho_{mn}}\,(\Delta_{sn} - \Delta_0)F(w_{mn})\,(1-\cos(k_0a_n))$$

or

$$\frac{e^{-jk_0\rho_{mn}}}{-jk_0\rho_{mn}}\,(\Delta_{sn} - \Delta_0)F(w_{mn})(k_0a_n)J_1(k_0a_n) \quad \text{for } m \neq n \tag{13a}$$

with $\rho_{mn} = \rho_{Bn}$ and $w_{mn} = w_{2n}$ and

$$C_{mn} = 1 + (\Delta_{sn} - \Delta_0)(1 - e^{-jk_0a_n}) \qquad \text{for } m = n. \tag{13b}$$

For $m = 1$ to N and $n = 1$ to N, $[C_{mn}]$ is a square matrix. The inverse of $[C_{mn}]$ exists. Hence, the vertical electric fields on the isolated surface can be obtained and

$$[E_n] = [C_{mn}]^{-1}[E^0_m]. \tag{14}$$

The scattered field due to the surface inhomogeneity at any point outside the surface can then be evaluated from (8) or its discretized form

$$E^s_{z1}(B) = \sum_{n=1}^{N} E_n\frac{e^{-jk_0\rho_{Bn}}}{jk_0\rho_{Bn}}\,(\Delta_{sn} - \Delta_0) \cdot F(w_{2n})\,(1-\cos(k_0a_n)) \tag{15a}$$

with the use of the first-order approximation of (11a) or, alternatively

$$E^s_{z1}(B) = \sum_{n=1}^{N} E_n\frac{e^{-jk_0\rho_{Bn}}}{jk_0\rho_{Bn}}\,(\Delta_{sn} - \Delta_0) \cdot F(w_{2n})(k_0a_n)J_1(k_0a_n) \tag{15b}$$

with the use of the physical optics approximation of (11b).

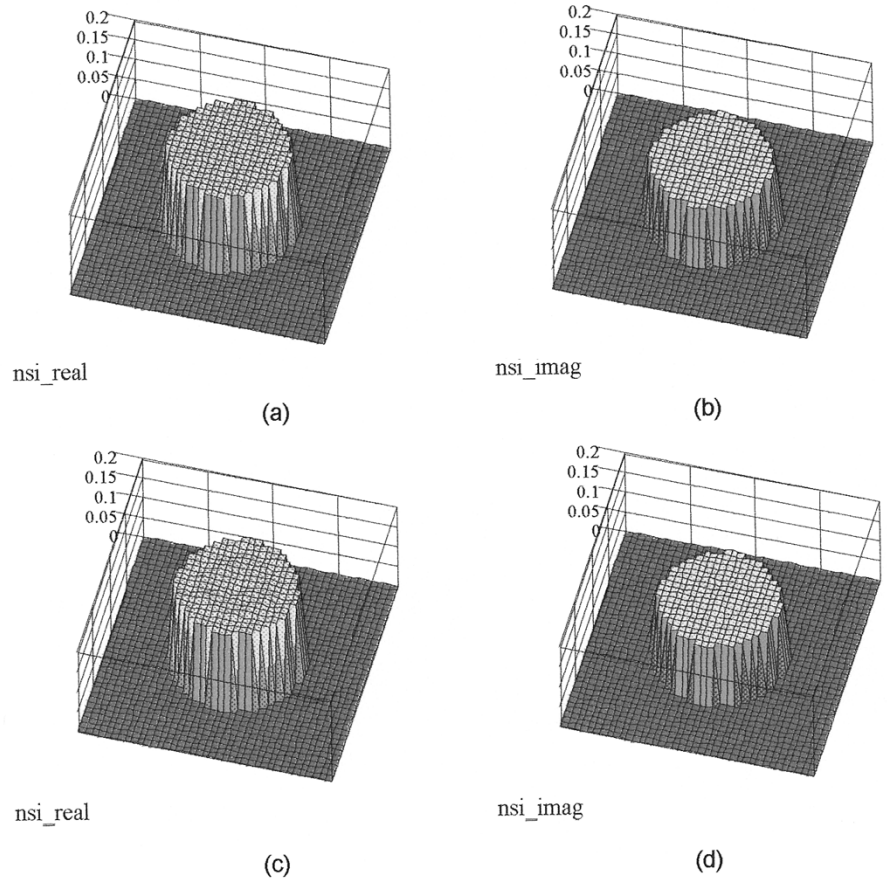

Fig. 3. The exact distributions of the (a) real part and (b) imaginary part of the normalized surface impedance of a dry ground with $\varepsilon_r = 4$ and $\sigma = 0.001$ S/m or $\Delta_s(P) = 0.184\,527 + j0.140\,076$ and the reconstructed distributions of the (c) real part and (d) imaginary part of the normalized surface impedance.

III. Formulation of the Inverse Problem of Radiowave Propagation Over an Isolated Surface

A. Measurement Configuration

In order to reconstruct the image of an isolated surface, which is assumed to be inaccessible otherwise, a number of measurements of scattered fields around the isolated surface are required to be made when the surface is illuminated sequentially with a number of waves from different directions. The arrangement is similar to that used in X-ray tomography or microwave tomography [49], [50]. It is made in such a way that "multiviews" of the isolated surface can be created. For simplicity, it is assumed that a total of K antennas are used. Each antenna is able to transmit and/or receive at a given time. The antennas are placed on a circle of diameter D enclosing the isolated surface with equal spacing at B_j for $j = 1$ to K, as shown in Fig. 2(b). Each of the K antennas will transmit in turn and receive in turn. This will generate "multiviews" of the isolated surface and enable the measurements of the scattered fields in K different "view angles" to be made. When the ith antenna acts as a transmitting antenna, the measurements of the scattered fields at K fixed points B_j for $j = 1$ to K are denoted as $E_{z1}^{s,\mathrm{meas}(i,j)}$ for $i = 1$ to K.

B. Iterative Reconstruction Algorithm

The task of the image reconstruction is to find the distribution of $\Delta_s(P)$ on the isolated surface which produces the same scattered fields as $E_{z1}^{s,\mathrm{meas}(i,j)}$ at the same point B_j with the same transmitting position i for $i = 1$ to K and $j = 1$ to K. Since the number of measurements taken is not generally equal to the number of unknowns Δ_{sn} for $n = 1$ to N, an exact solution of $\Delta_s(P)$ can hardly be found. The task may be reduced to find an approximated solution of $\Delta_s(P)$, which minimizes the difference between the measured scattered fields $E_{z1}^{s,\mathrm{meas}(i,j)}$ and the estimated scattered fields, denoted as $E_{z1}^{s,est(i,j)}$ for $i = 1$ to K and $j = 1$ to K as a result of the estimated distribution of $\Delta_s(P)$ for the same transmitting and receiving conditions. This can be made in an iterative manner to minimize the square of the second-order norms of the errors between the estimated and measured scattered electric fields, or the cost function [55] defined as

$$F_{\mathrm{cost}}(\Delta_s^{est}) = \sum_{i=1}^{K}\sum_{j=1}^{K} |\Psi_{ij}|^2 = \sum_{i=1}^{K}\sum_{j=1}^{K} \left| E_{z1}^{s,meas(i,j)} - E_{z1}^{s,est(i,j)} \right|^2. \quad (16)$$

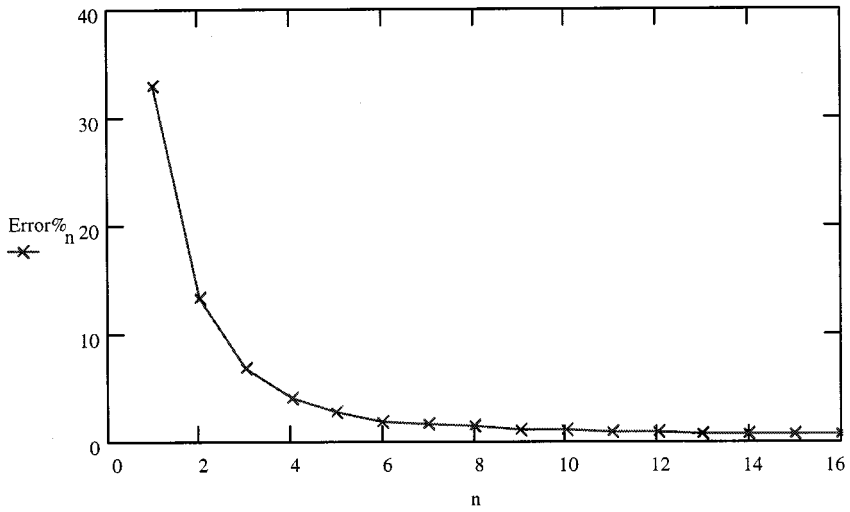

Fig. 4. Percentage error of the iterative process against the number of iterations for the dry ground surface.

There exist a number of mathematical techniques that can be used in the minimization of (16) [55], [56]. Here, the steepest descent-based minimization technique is used. The search for the approximated solution starts with a guessed distribution of $\Delta_s^{est0}(P)$ or a set of guessed values of Δ_{sn}^{est0} for $n = 1$ to N in the discretized form. The complex updating direction d_n, which combines the directions for changes in real and imaginary parts, for each Δ_{sn}^{est0} will then be determined so as to reduce the error in (16). The direction is chosen as the negative direction of the complex slope when the real and imaginary parts of Δ_{sn}^{est} are varied, respectively, from Δ_{sn}^{est0}. Using the differentiation procedures described in [55], it can be derived that

$$d_n = -\sum_{i=1}^{K}\sum_{j=1}^{K} 2\Psi_{ij}\frac{\partial \Psi_{ij}^*}{\partial \mathrm{Re}(\Delta_{sn})} \tag{17}$$

where * denotes the complex conjugate of the function. Hence, an updated value of Δ_{sn}^{est} would become

$$\Delta_{sn}^{est} = \Delta_{sn}^{est0} + \beta d_n \tag{18}$$

where β is the step length determined from the minimization of the error function

$$f(\beta) = F_{\cos t}(\Delta_{sn}^{est0} + \beta d_n). \tag{19}$$

It can be shown that

$$\beta = \frac{\mathrm{Re}\left[\sum_{i=1}^{K}\sum_{j=1}^{K}\Psi_{ij}\left(\sum_{n=1}^{N}(-d_n)\frac{\partial \Psi_{ij}}{\partial \mathrm{Re}(\Delta_{sn})}\right)^*\right]}{\sum_{i=1}^{K}\sum_{j=1}^{K}\left|\sum_{n=1}^{N}(-d_n)\frac{\partial \Psi_{ij}}{\partial \mathrm{Re}(\Delta_{sn})}\right|^2}. \tag{20}$$

When d_n and β are obtained, the values of Δ_{sn}^{est} can be updated using (18), the iterative process will then be continued. The overall error estimation in each iteration can be made using the following normalized root mean square (rms) error function:

$$F_{\mathrm{Error}} = \sqrt{\frac{\sum_{i=1}^{K}\sum_{j=1}^{K}\left|E_{z1}^{s,\,\mathrm{meas}(i,j)} - E_{z1}^{s,\,est(i,j)}\right|^2}{\sum_{i=1}^{K}\sum_{j=1}^{K}\left|E_{z1}^{s,\,\mathrm{meas}(i,j)}\right|^2}}. \tag{21}$$

The iteration terminates when the overall error measured using (21) meets the permitted error requirement or the required number of iterations is reached.

IV. Numerical Results

The validity of the image reconstruction technique described in Section III will now be illustrated using the four following isolated ground features: 1) dry ground; 2) wet ground; 3) dry–wet mixed ground surface; and 4) dry ground with a central water pool. In each case, the isolated surface is considered to be surrounded by sea water and assumed to be confined within a circle of diameter of 300 m. The circular surface is divided into five rings with 4, 12, 20, 28, and 36 segments, respectively, from the innermost to the outermost rings, as shown in Fig. 2(a). Thus, there are a total of 100 cells of equal area, with cells being numbered from 1 to 100 anticlockwise from the inner ring to the outer rings. The transmitting and receiving antennas are located at 18 fixed points along a circle with a diameter of $D = 450$ m. The frequency of operation is taken to be 1 MHz. At 1 MHz, the normalized surface impedance of sea water with a relative dielectric constant $\varepsilon_r = 80$ and conductivity $\sigma = 4$ S/m is $\Delta_0 = 0.002\,637 + j0.002\,634$. The measured scattered fields in Section III, are obtained by using (15a) with the known distribution of ground properties for each case. Initial guessed values of Δ_{sn} required in the iteration process are taken to be

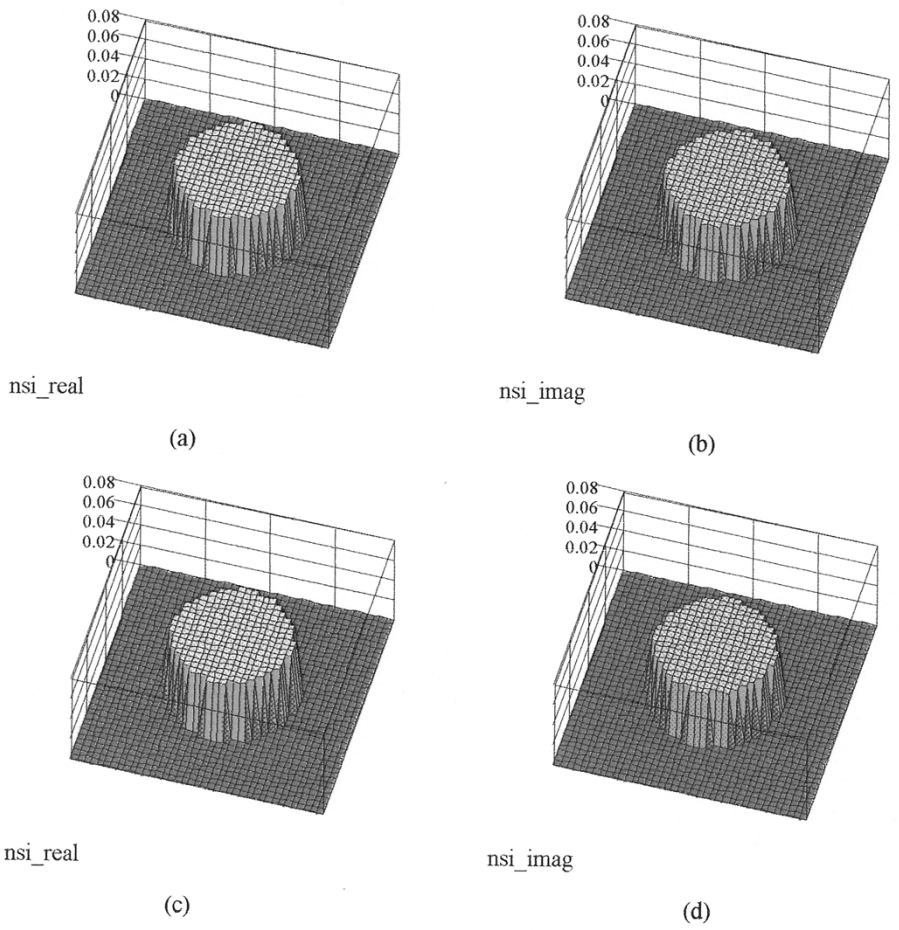

Fig. 5. The exact distributions of the (a) real part and (b) imaginary part of the normalized surface impedance of a wet ground with $\varepsilon_r = 10$ and $\sigma = 0.01$ S/m or $\Delta_s(P) = 0.054\,239 + j0.051\,025$ and the reconstructed distributions of the (c) real part and (d) imaginary part of the normalized surface impedance.

Δ_0 for all cases, and the errors of reconstruction are evaluated using the definition

$$\text{Error} = \sqrt{\frac{\sum_{n=1}^{N} |\Delta_{sn} - \Delta_{sn}^{\text{exact}}|^2}{\sum_{n=1}^{N} |\Delta_{sn}^{\text{exact}}|^2}}. \tag{22}$$

A. Dry Ground Surface

The first isolated surface used to test the algorithm is dry ground having a relative dielectric constant of $\varepsilon_r = 4$ and conductivity $\sigma = 0.001$ S/m, giving a normalized surface impedance $\Delta_s(P) = \Delta_{sn} = 0.184\,527 + j0.140\,076$. The distributions of the real and imaginary parts of Δ_{sn}, Re(Δ_{sn}) and Im(Δ_{sn}), are shown in Fig. 3(a) and (b), respectively. Using the reconstruction algorithm described in Section III, the reconstructed distributions of Re(Δ_{sn}) and Im(Δ_{sn}) after 16 iterations are shown in Fig. 3(c) and (d), respectively. The distributions of both Re(Δ_{sn}) and Im(Δ_{sn}) are well reconstructed with an error of 0.7% evaluated using (22). The error of reconstruction for each iteration is shown in Fig. 4. The error reduces monotonically as the number of iteration increases, and an error less than 1% can be achieved after 12 iterations.

B. Wet Ground Surface

The isolated wet ground used for the reconstruction has a relative dielectric constant of $\varepsilon_r = 10$ and conductivity $\sigma = 0.01$ S/m for which the normalized surface impedance is $\Delta_s(P) = \Delta_{sn} = 0.054\,239 + j0.051\,025$. The distributions of Re(Δ_{sn}) and Im(Δ_{sn}) are shown in Fig. 5(a) and (b), respectively, and the reconstructed distributions of Re(Δ_{sn}) and Im(Δ_{sn}) after 16 iterations in Fig. 5(c) and (d), respectively. Again, the distributions of both Re(Δ_{sn}) and Im(Δ_{sn}) are well reconstructed. The error of reconstruction is very similar to that for the dry ground shown in Fig. 4, with the error falling below 1% after 12 iterations.

C. Dry–Wet Mixed Ground Surface

The isolated ground surfaces in cases A and B above are each homogeneous. A combination of dry and wet ground areas generates an artificial mixed inhomogeneous ground surface. For the half-dry and half-wet combination, the distributions of Re(Δ_{sn}) and Im(Δ_{sn}) are shown in Fig. 6(a) and (b), respectively. The reconstructed distributions of Re(Δ_{sn}) and Im(Δ_{sn}) after 16 iterations are shown in Fig. 6(c) and (d), respectively,

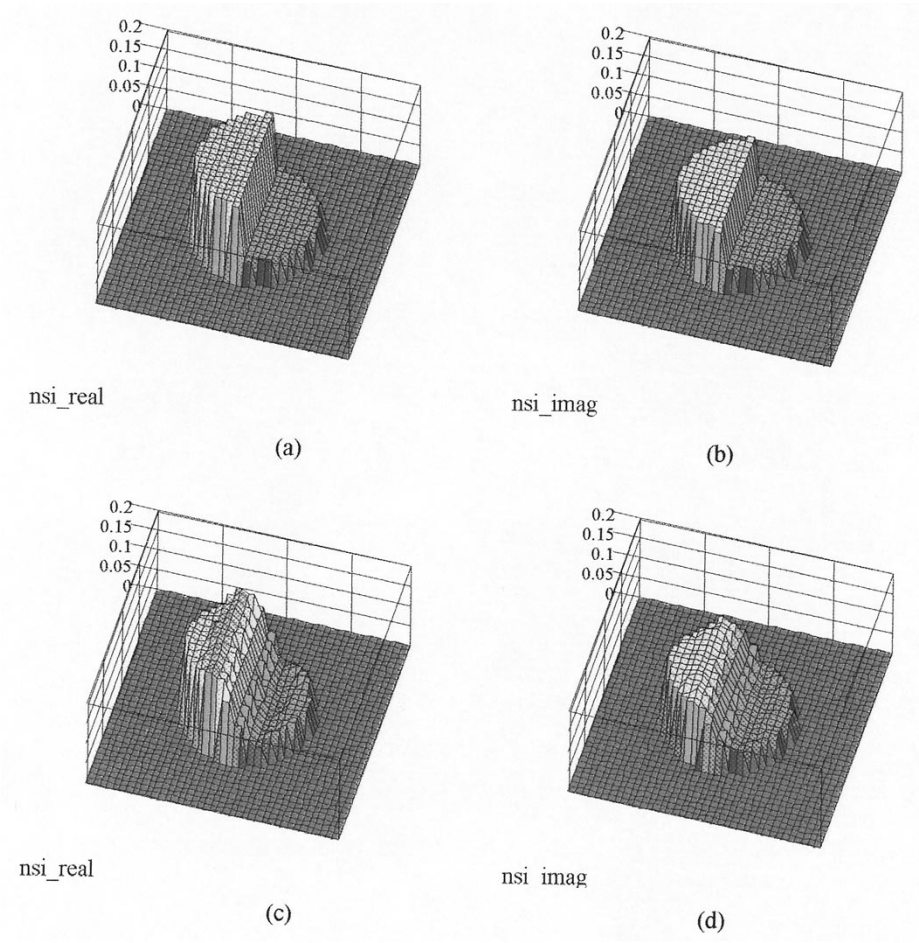

Fig. 6. The exact distributions of the (a) real part and (b) imaginary part of the normalized surface impedance of a half dry and half wet mixed surface and the reconstructed distributions of the (c) real part and (d) imaginary part of the normalized surface impedance.

with an error of 13.7%. Due to the sharp change in the normalized surface impedance between the dry and wet ground areas, the error of reconstruction converges slowly. A larger number of iterations is needed to achieve an improved accuracy. The spatial "low-pass" filtering effect can be observed from the reconstructed distributions. The sharp change has been smoothed. However, the image of the half dry and half wet ground can be seen from either the distribution of $\mathrm{Re}(\Delta_{sn})$ or $\mathrm{Im}(\Delta_{sn})$.

The distributions of $\mathrm{Re}(\Delta_{sn})$ and $\mathrm{Im}(\Delta_{sn})$ shown in Fig. 6(c) and (d) are obtained without using *a priori* information of the ground properties. If the ground surface is known to be either wet or dry, this information can be fed into the algorithm after a number of iterations. For instance, if the information is fed into the algorithm after 16 iterations, the algorithm is able to reconstruct the exact distributions of both $\mathrm{Re}(\Delta_{sn})$ and $\mathrm{Im}(\Delta_{sn})$ after one further iteration, which are the same as those shown in Fig. 6(a) and (b). The error evaluated using (22) is then effectively zero.

D. Dry Ground with a Central Water Pool

The discontinuity in ground properties in case C above occurs in the azimuthal direction of the isolated surface. In this present case, the algorithm is to be tested for a discontinuity in the radial direction. The isolated surface is composed of a water pool, with a diameter of 120 m at the center and dry ground in the rest of the area. The electrical properties of water are taken to have a relative dielectric constant of $\varepsilon_r = 80$ and conductivity $\sigma = 0.1$ S/m, giving a normalized surface impedance of $\Delta_s(P) = 0.017\,029 + j0.016\,28$ at 1 MHz. The dry ground has the same properties as that in Case A having a relative dielectric constant of $\varepsilon_r = 4$ and conductivity $\sigma = 0.001$ S/m, or a normalized surface impedance of $\Delta_s(P) = 0.184\,527 + j0.140\,076$. The distributions of $\mathrm{Re}(\Delta_{sn})$ and $\mathrm{Im}(\Delta_{sn})$ of the isolated surface are shown in Fig. 7(a) and (b), respectively. The reconstructed distributions of $\mathrm{Re}(\Delta_{sn})$ and $\mathrm{Im}(\Delta_{sn})$ after 16 iterations are shown in Fig. 7(c) and (d), respectively, with an error of 13.2%. Again, due to the sharp change in the normalized surface impedance between the water and dry ground, the reconstruction converges slowly. The spatial "low-pass" filtering effect can also be observed from the reconstructed distributions, with the sharp change appearing in smoothed form. However, the image of this circular water pool in the dry ground can be seen clearly from either the distribution of $\mathrm{Re}(\Delta_{sn})$ or $\mathrm{Im}(\Delta_{sn})$.

Again, if the ground surface is known to be either dry or full of water, this *a priori* information can be fed into the algorithm. When this is done after 16 iterations, the algorithm is able to reconstruct the exact distributions of both $\mathrm{Re}(\Delta_{sn})$ and $\mathrm{Im}(\Delta_{sn})$, as shown in Fig. 7(a) and (b), respectively, after one further iteration.

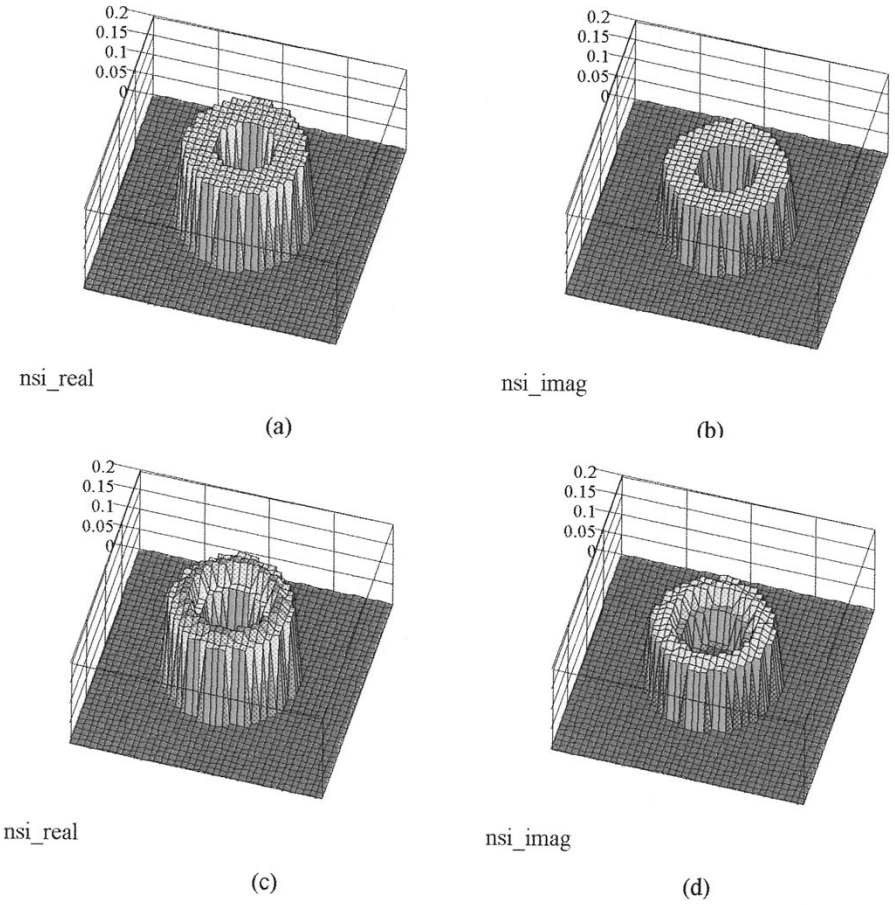

Fig. 7. The exact distributions of the (a) real part and (b) imaginary part of the normalized surface impedance of a dry land with a center water pool and the reconstructed distributions of the (c) real part and (d) imaginary part of the normalized surface impedance.

V. Conclusion

In this paper, a technique for the tomographic imaging of isolated ground surfaces is illustrated for the first time using both the theory ground-wave propagation and the measurements of scattered fields around the isolated surfaces with different transmitting positions. These images are generated from the reconstructed distributions of the real and imaginary parts of the normalized surface impedance on the isolated surfaces.

It has been demonstrated through the simulation of four different ground features that the distributions of both real and imaginary parts of the normalized surface impedance can be reconstructed using the minimization technique, and the steepest descent search method. The reconstruction process has made use of the first order approximation of the spherical harmonic expansion of $\exp(-jk_0\rho_2)/\rho_2$, which is shown to be effective. This could, however, be improved slightly if the physical optics approximation is used. The initial guessed values may be important in finding a quick solution. However, the algorithm has been shown to be able to produce the distributions of normalized surface impedance with a small number of iterations, even using the normalized surface impedance of sea water as the initial guessed values. But, the *a priori* information has proved useful in the reconstruction process and it can become important when a highly accurate distribution is to be obtained with a small number of iterations.

The study presented in this paper shows a new application of the theory of ground wave propagation. It may be useful in ground surface mapping, remote sensing, target positioning and monitoring, and navigation.

Acknowledgment

The author would like to thank the reviewers for their comments and, in particular, for their suggestion of the physical optics approximation leading to (11b), which may be used as an alternative to (11a). The author would also like to thank Prof. T. S. M. Maclean for his comments and suggestions toward the final preparation of this paper.

References

[1] J. R. Wait, "The ancient and modern history of EM ground wave propagation," *IEEE Antennas Propagat. Mag.*, vol. 40, pp. 7–22, Oct. 1998.

[2] ——, "Recent analytical investigations of electromagnetic ground wave propagation over inhomogeneous earth models," *Proc. IEEE*, vol. 62, pp. 1061–1071, Aug. 1974.

[3] A. Sommerfield, "Uber die ausbeitung der wellen in der drahtlosen telegraphie," *Annalen den Physik*, vol. 81, pp. 1135–1153, 1926.

[4] ——, *Patial Differential Equations in Physics*. New York: Academic, 1949.
[5] B. Van del Pol, "Theory of the reflection of the light from a point source by a finite conducting flat mirror with an application to radiotelegraphy," *Physica*, vol. 2, pp. 843–853, 1935.
[6] K. A. Norton, "The propagation of radio waves over the surface of the earth and in the upper atmosphere," *Proc. IRE*, vol. 25, pp. 1203–1236, 1937.
[7] J. R. Wait, *Electromagnetic Waves in Stratified Media*. New York: Pergamon, 1962.
[8] ——, "Electromagnetic surface waves," in *Advances in Radio Research*, J. A. Saxton, Ed. New York: Academic, 1964, vol. 1, pp. 157–217.
[9] A. Banos, *Dipole Radiation in the Presence of a Conducting Half-Space*. Oxford, U.K.: Pergamon, 1966.
[10] R. J. King, "Electromagnetic wave propagation over a constant impedance plane," *Radio Sci.*, vol. 4, pp. 255–268, 1969.
[11] R. J. King and J. R. Wait, "Electromagnetic groundwave propagation theory and experiment," *Symp. Math.*, vol. 18, pp. 107–207, 1976.
[12] G. N. Watson, "The diffraction of electric waves by the earth," *Proc. Roy. Soc. London*, pt. A, vol. 95, pp. 83–99, 1918.
[13] ——, "The transmission of electric waves round the earth," *Proc. Roy. Soc. London*, pt. A, vol. 95, pp. 546–563, 1919.
[14] V. A. Fock, "Diffraction of radio waves around the Earth's surface," *J. Physics (Moscow)*, vol. 9, pp. 256–266, 1945.
[15] H. Bremmer, *Terrestrial Radio Waves*. New York: Elsevier, 1949.
[16] V. A. Fock, *Electromagnetic Diffraction and Propagation Problems*. Oxford, U.K.: Pergamon, 1965.
[17] D. A. Hill and J. R. Wait, "Ground wave attenuation function for a spherical earth with arbitrary surface impedance," *Radio Sci.*, vol. 15, no. 3, pp. 637–673, 1980.
[18] E. Feinberg, "On the propagation of radio wave along an imperfect surface—Parts I, II," *J. Physics (USSR)*, vol. VIII, no. 6, pp. 317–330, 1944.
[19] ——, "On the propagation of radio wave along an imperfect surface—Part III," *J. Physics (USSR)*, vol. IV, no. 6, pp. 1–6, 1945.
[20] G. D. Monteath, "Application of the compensation theorem to certain radiation and propagation problems," *Proc. Inst. Elect. Eng.*, vol. 98, pp. 23–30, 1951.
[21] J. R. Wait, "Mixed-path groundwave propagation, 1-short distance," *J. Res. Nat. Bur. Stand.*, vol. 57, no. 1, pp. 1–15, 1956.
[22] J. R. Wait and J. Householder, "Mixed-path groundwave propagation, 2-larger distance," *J. Res. Nat. Bur. Stand.*, vol. 59, pp. 19–26, 1957.
[23] Z. Godzinski, "The theory of groundwave propagation over inhomogeneous earth," *Proc. IEEE*, pt. C, vol. 105, pp. 448–464, 1958.
[24] J. R. Wait, "On the theory of mixed-path ground wave propagation on a spherical earth," *J. Res. Nat. Bur. Stand.*, pt. D, vol. 65, pp. 401–410, 1961.
[25] ——, "Oblique propagation of ground waves across coastline—Part I," *J. Res. Nat. Bur. Stand.*, vol. 67, no. 6, pp. 617–624, 1963.
[26] ——, "Oblique propagation of ground waves across coastline—Part II," *J. Res. Nat. Bur. Stand.*, vol. 67, no. 6, pp. 625–630, 1963.
[27] ——, "Oblique propagation of ground waves across coastline—Part III," *J. Res. Nat. Bur. Stand.*, vol. 68, no. 3, pp. 291–296, 1964.
[28] J. R. Wait and K. P. Spies, "Propagation of radiowaves past a coastline with a gradual change of surface impedance," *IEEE Trans. Antennas Propagat.*, vol. AP-12, pp. 570–575, Sept. 1964.
[29] R. J. King and S. W. Maley, "Model experiments on propagation of groundwaves across an abrupt boundary at oblique incidence," *Radio Sci.*, vol. 1, pp. 111–115, 1966.
[30] R. J. King, S. W. Maley, and J. R. Wait, "Groundwave propagation along the three-section mixed paths," *Proc. Inst. Elect. Eng.*, vol. 113, no. 5, pp. 747–751, 1966.
[31] R. J. King and W. I. Tsukamoto, "Groundwave propagation across semi-infinite strips and island on a flat earth," *Radio Sci.*, vol. 1, no. 7, pp. 775–788, 1966.
[32] E. C. Field Jr., "Low-frequency groundwave propagation over narrow terrain features," *IEEE Trans. Antennas Propagat.*, vol. AP-30, pp. 831–836, Sept. 1982.
[33] R. J. King, S. W. Maley, and J. R. Wait, "Experimental and theoretical studies of propagation of groundwave across mixed-paths," in *Electromagnetic Wave Theory*, J. Brown, Ed. New York: Pergamon, 1967, pp. 217–224.
[34] S. Christiansen and T. Larsen, "Numerical application of the compensation theorem to mixed-path propagation problems," *Radio Sci.*, vol. 2, no. 12, pp. 1471–1479, 1967.
[35] J. R. Wait and K. P. Spies, "Integral equation approach to the radiation from a vertical antenna over an inhomogeneous ground plane," *Radio Sci.*, vol. 5, pp. 73–79, 1970.
[36] G. de Jong, "Electromagnetic wave propagation over an inhomogeneous flat earth: Two-dimensional integral equation formulation," *Radio Sci.*, vol. 10, no. 11, pp. 925–933, 1975.
[37] D. A. Hill and J. R. Wait, "HF radio wave transmission over sea ice and remote sensing possibilities," *IEEE Trans. Geosci. Remote Sensing*, vol. GRS-19, pp. 204–209, Oct. 1981.
[38] M. Yamashita and K. Taguchi, "Phase disturbance of 100-kHz groundwaves by a circular island in the open sea," *IEEE J. Oceanic Eng.*, vol. OE-6, pp. 26–31, Jan. 1981.
[39] G. A. Hufford, "An integral equation approach to the problem of wave propagation over an irregular surface," *Q. J. Appl. Math.*, vol. 9, no. 4, pp. 391–404, 1952.
[40] R. H. Ott, "An alternative integral equation for propagation over irregular terrain—Part 2," *Radio Sci.*, vol. 5, no. 5, pp. 767–771, 1970.
[41] R. H. Ott and L. A. Berry, "An alternative integral equation for propagation over irregular terrain—Part 2," *Radio Sci.*, vol. 6, no. 4, pp. 429–435, 1971.
[42] R. H. Ott, "RING: An integral equation algorithm for HF-VHF radio wave propagation over irregular, inhomogeneous terrain," *Radio Sci.*, vol. 27, no. 6, pp. 867–882, 1992.
[43] Z. Wu, T. S. M. Maclean, D. J. Bagwell, and M. J. Mehler, "Propagation over an inhomogeneous irregular surface," *Radio Sci.*, vol. 23, no. 1, pp. 33–40, 1988.
[44] ——, "Radiowave propagation in the presence of finite width knife-edges," *Radio Sci.*, vol. 24, no. 3, pp. 361–368, 1989.
[45] G. D. Monteath, *Application of Electromagnetic Reciprocity Principle*. New York: Pergamon, 1973.
[46] R. Mittra, "A vector form of compensation theorem and its application to boundary value problems," *Appl. Sci. Res. B*, vol. 11, pp. 26–42, 1964.
[47] J. A. Stratton, *Electromagnetic Theory*. New York: McGraw-Hill, 1941.
[48] A. Ishimaru, *Electromagnetic Wave Propagation, Radiation, and Scattering*. Englewood Cliffs, NJ: Prentice-Hall, 1991, pp. 144–146, 565–566.
[49] A. C. Kak and M. Slaney, *Computerised Tomographic Imaging*. New York: IEEE Press, 1988.
[50] J. C. Bolomey and C. Pichot, "Microwave tomography: From theory to practical imaging system," *Int. J. Imaging Syst. Technol.*, vol. 2, pp. 144–156, 1990.
[51] T. S. M. Maclean and Z. Wu, *Radiowave Propagation Over Ground*. London, U.K.: Chapman Hall, 1993.
[52] Z. Wu and T. S. M. Maclean, *Radiowave Propagation Over Ground Software*. London, U.K.: Chapman Hall, 1998.
[53] J. H. Richmond, "Scattering by a dielectric cylinder of arbitrary cross section shape," *IEEE Trans. Antennas Propagat.*, vol. AP-13, pp. 334–341, May 1965.
[54] R. F. Harrington, *Time-Harmonic Electromagnetic Fields*. New York: McGraw-Hill, 1961, pp. 289–292.
[55] P. Neittaanmaki, M. Rudnicki, and A. Savini, *Inverse Problems and Optimal Design in Electricity and Magnetism*. Oxford, U.K.: Clarendon Press, 1996.
[56] W. H. Press, S. A. Teukolsky, W. T. Vetterling, and B. P. Flannery, *Numerical Recipes in C*, 2nd ed. Cambridge, U.K.: Cambridge Univ. Press, 1992.

Zhipeng Wu (M'95) received the B.Sc. degree from the Northeast Institute of Technology, Shenyang, China, in 1983, and the Ph.D. degree from the University of Birmingham, Birmingham, U.K., in 1988, all in electrical engineering.

From 1988 to 1991, he was a Research Fellow in the School of Electronic and Electrical Engineering, University of Birmingham, U.K. In 1992, he joined the University of Manchester Institute of Science and Technology, U.K., where he is now a Senior Lecturer. His research interests include antenna modeling, radiowave propagation over ground, RF and microwave tomographic imaging, microwave measurement of superconducting and dielectric materials, and RF and microwave sensors for industrial applications.